Regulating Top-surface Graphene Growth by "Gettering" Carbon Diffusion at Backside of the Copper Foil

Irfan H. Abidi,[a] Yuanyue Liu,[b,c] Jie Pan,[d] Abhishek Tyagi,[a] Minghao Zhuang, [a] Qicheng Zhang,[a] Aldrine A. Cagang,[a] Lu-Tao Weng,[a,e] Ping Sheng,[d] William A. Goddard [b] and Zhengtang Luo[*,a]

[a]Department of Chemical and Biomolecular Engineering, Hong Kong University of Science and Technology, Clear Water Bay, Kowloon, Hong Kong

[b]Materials and Process Simulation Center, [c]The Resnick Sustainability Institute, California Institute of Technology, Pasadena, California 91125, United States

[d]Department of Physics and William Mong Institute of Nano Science and Technology, Hong Kong University of Science and Technology, Kowloon, Hong Kong

[e]Materials Characterization and Preparation Facility, The Hong Kong University of Science and Technology, Clear Water Bay, Hong Kong

Abstract

We reported a simple and practical strategy that enables us to control the nucleation density and growth kinetics for graphene grown on the top-surface of metal substrate through gettering the carbon source on the backside of the flat Cu foil, during chemical vapor deposition (CVD). Hitherto, for CVD graphene grown on a flat Cu foil, merely top-surface-based growth mechanism has been emphasized, while the effects from diffused carbon and graphene layer formed on the backside of the Cu foil is normally overlooked. Our systematic experimental findings indicated that graphene grown on the backside, governs the carbon diffusion through the bulk Cu, thus strongly dominate nucleation process on the top surface. This understanding steers us to devise a strategy of regulating carbon diffusion to the top surface by using a "getter" substrate such as nickel for carbon at backside of the Cu foil. Depth profiling of the nickel substrate, along with Density Functional Theory (DFT) calculation, verifies the gettering role of nickel support. Implementing, backside carbon gettering (BCG) approach to single-crystal graphene growth resulted in lowering of the nucleation density by two orders of magnitude, enabling growth of single-crystal domains of ~ 6 mm lateral size on untreated Cu foil. Finally, we demonstrate the growth of large area polycrystalline SLG, free of unwanted MLG domains, with significantly improved the field-effect mobility of ~ 6800 $cm^2V^{-1}s^{-1}$ and 97.7% optical transmittance. Our approach provides an unusual methodology for control in chemical vapor deposition of 2D materials.

Introduction

Graphene brings the aspiration for the worldwide researchers to achieve highly efficient and flexible electronic and optoelectronic devices, owing to its exceptional optical and electronic mobility characteristics.[1] Beyond the mechanical exfoliation method, which is limited in terms of size and uniformity, chemical vapor deposition (CVD) on transition metals emerges as a practical and scalable method to meet the ever increasing demand of uniform and large area graphene.[2, 3] Among all the substrates, copper (Cu) provides better control for uniformity and number of layers of graphene through self-limiting surface mechanism.[4] Although, considerable success have been made to grow high-quality CVD graphene, yet efforts required to accomplish the goal of obtaining large, uniform, and defect free flat single layer graphene (SLG). The major challenges are to deal with defects

such as grain boundaries and unwanted multilayer graphene (MLG) patches beneath the monolayer graphene, acting as electron scattering barriers that severely affect the electrical as well as optical performances.[5-7] In the last few years, numerous efforts underwent to develop large, single crystal graphene as a strategy to circumvent the adverse effect of grain boundaries, hitherto limited to smaller size within practical time and growth conditions.[8-12] Moreover, the existence of MLG patches persists in single crystal SLG growth, affecting the essence of this technique.[7, 10] Although, various approaches have been adopted to restrict the presence of MLG patches, particularly manipulating surface treatment,[13-15] re-solidifying[16] and varying composition of Cu foil,[17] or modifying the CVD process by introducing pulsed growth.[18] Nevertheless, these strategies are either unsuccessful to completely limit the MLG existence or worked only within constrained growth conditions and requiring extensive pretreatments. Therefore, devising a robust method to synthesize large-area uniform SLG, irrespective of growth conditions and surface treatment of Cu foil, is indispensable for scaling up its growth at the industrial level. On the other hand, the role of carbon diffusion from interior surface of Cu has been discussed for a few interesting configuration, such as pocket or deliberated gaps, during bi/multi-layer graphene (B/MLG) growth,[19-22] but seldom explored a flat Cu foil, notwithstanding, more practical and industrially viable configuration. Despite, the top surface of flat Cu foil has been considered solely responsible for bi- or multilayer graphene growth governing by two mechanisms; 1) adsorption-diffusion and 2) gas phase penetration.[23-26] Although most of the time graphene growth was observed on both sides of Cu foil,[7, 21, 27] see Table-1 supporting information. Moreover, enormous top surface based strategies are employed to control the nucleation density of graphene domains for large single-crystal graphene growth,[9, 10, 12, 28] ignoring the backside effect, which indeed has a wide spectrum of implementation. Therefore, exploring the backside carbon diffusion and its impression on the kinetics of graphene growth on the top side of flat Cu foil is indispensable for a full understanding of CVD process to obtain desired graphene structures.

In this work, we systematically studied the role of carbon diffusion on the growth mechanism of MLG domains as well as single crystal graphene, and redirected the growth using "gettering" process at the backside by replacing the support substrate for flat Cu foil. Our studies demonstrated the direct correlation between growth of graphene on the top surface and the graphene coverage on the backside of Cu foil that governs by the C species diffusion through bulk Cu, consistent to Cu pocket configuration.[19, 22] Later, we found this C diffusion can be restricted completely by "gettering" the accumulated carbon at the backside using a nickel support substrate. Finally, density function theory (DFT) calculations validate the role of nickel substrate that provides preferential sites for C species to bind as compared to the Cu surface. We implemented this unique backside carbon gettering (BCG) approach to alleviate the nucleation density of graphene domains as low as 6.11 nuclei/cm^2, which eventually leads to the growth of large size single crystal graphene domain for diameter reaches to ~ 6 mm. More importantly, with this method, high-quality single layer graphene was produced even without surface treatment, a major step towards industrial scale production. Our study provides new understanding of carbon gettering to synthesize uniform high-quality large area single crystal graphene for next generation electronic and optoelectronic devices.

Results and discussion

Figure 1a illustrates the configuration of Cu foil supported by a solid substrate in our CVD system. Herein, we intend to explore the influence of support substrate on the kinetics of graphene growth on both sides of Cu foil, as recent work has shown that the support substrate plays a crucial role for graphene growth on only backside.[29, 30] We carried out CVD growth on Cu foil resting on three different substrates (i) quartz (ii) Cu coated quartz (hereafter refer as "quartz(Cu)") and (iii) nickel, shown inset of Figure 1(b). Figure 1b illustrates the XRD spectra of quartz(Cu), showing the successful fusion of Cu on quartz during several CVD cycles,[31] and Ni substrate. Figure1c-h depict the top and back side of the Cu foil after 5 minutes of CVD growth using quartz (c,f), quartz(Cu) (d,g) and nickel (e,h), as supporting substrate, using a reported visualization method.[32] The obtained samples, are designated as Cu/quartz, Cu/quartz(Cu) and Cu/nickel, respectively, henceforth. On the top surface, the graphene coverages are similar at present growth conditions and reach ~80% coverage within 5 minutes of CVD growth, shown in Figure 1c-e. Nevertheless, the growth behaviors on the backside distinct, as shown in Figure 1f-h and supplementary Figure S1. For instance, Figure 1f reveals the graphene coverage on the backside was <20% for Cu/quartz after 5 minutes of growth, significantly slower compared to the top surface (~80%). While, Figure 1g illustrates the graphene coverage reaches to above 40% for Cu/quartz(Cu), relatively faster than Cu/quartz. On the contrary, we did not observe any graphene growth for Cu/nickel as shown in Figure 1h, and it persists even though we prolonged the growth for 3 hours (supplementary Figure S2). These observations reflect the indispensable role of the support substrate in CVD growth kinetics, hitherto overlooked. For Cu/quartz and Cu/quartz(Cu), the differences in growth rate can be explained with respect to the limited diffusion of gasses through the micro/nano gaps present between Cu foil and the underlying substrate. Such limited diffusion is evident from graphene distribution on the backside of Cu foil, showing high density at edges and low concentration at the middle part (supplementary Figure S3). The asymmetric growth rate on top and backside surface of Cu foil is similar to that observed for two surfaces of Cu pocket configuration.[19, 20, 22] Furthermore, the amplified growth rate *via* quartz(Cu) substrate can be explained considering the additional supply of catalyst (Cu evaporated on quartz) for accelerated dehydrogenation of methane gas, which eventually increases graphene growth rate.[30, 33]

Figure 2a-c illustrates the optical images of graphene film grown on the top surface of Cu foil after 60 minutes of CVD growth and transferred to SiO_2/Si substrate. The contrast under an optical microscope allows us to differentiate between single layer graphene (SLG) and multilayer graphene (MLG) domains,[34] as pointed out with arrows. We did not find noticeable MLG domains for Cu/nickel growth, rather the film consists of uniform SLG, as shown in Figure 2c, in contrast to the presence of MLG for other two Cu/quartz and Cu/quartz(Cu) samples. This is further confirmed by the Raman spectra acquired from multiple spots, presenting the presence of MLG patches for graphene growth on Cu/quartz and Cu/quartz(Cu), whereas only SLG film were observed for Cu/nickel, evaluated based on typical intensity ratio of G and 2D bands for SLG and MLG (inset of Figure 2a-c).[35]

Figure 2d-f plotted MLG domain size present on the top surface of Cu foil against CVD growth time, along with the percentage of Cu surface exposed (100 - graphene coverage (%)) at back side of the Cu foil. Previously, surface exposed at the top surface of Cu foil is considered as the main origin for continual growth of bi-multilayer graphene under the SLG,[23, 25] and growth ceased once after the top surface is completely covered with graphene,

due to the self-limiting effect of Cu.[19] However, Figure 2d shows MLG domains continue to grow larger even after the complete coverage of the top surface, also evident from optical images shown in supplementary Figure S4. Instead, we found that growth kinetics of MLG domain correlates closely with the percentage coverage on the backside of Cu foil, as indicated in Figure 2e where the growth of MLG domains almost ceased completely after 20 minutes of CVD growth, concurring with complete coverage of graphene on the backside. Such correlation is also demonstrated by Cu/nickel sample, as shown in Figure 2f. This correlation is consistent with previous observation that carbon diffusion from back to the top surface, previously reported for BLG growth for Cu enclosure (pocket) configuration.[19, 20] In our case, we proposed that carbon precursors diffuses through the inevitable gaps between Cu foil and support substrate, subsequently dehydrogenate on backside of Cu foil to give C active species, which eventually diffuse through the bulk Cu to nucleate MLG domains underneath the SLG layer on top side of Cu foil. These active C continues to diffuse through the Cu until a threshold concentration reached necessary to start graphene nucleation on the backside.[36] Accordingly, once the graphene completely covers the backside of Cu foil (Figure 2e), it passivates the catalytic surface for further dehydrogenation of carbon precursors and also acts as a diffusion barrier,[23] resulting in termination of carbon diffusion through the bulk Cu, eventually leading to the cessation of the continual growth of MLG domains even for prolonged CVD growth. On the other hand, for the Cu/nickel configuration, the absence of graphene on the backside of Cu foil indicates the lack of carbon species available for graphene nucleation at the subsequent surface. This is consistent with the absence of MLG domains on the top surface (Figure 2c), due to the unavailability of C species for bulk diffusion. We believe nickel plays an important role in creating carbon deficiency in the vicinity of back Cu surface. Convincingly, we found that MLG growth on the top surface of Cu foil originates from the bottom (backside), which can be suppressed by terminating the carbon supply to the top surface.

As a proof of concept, we extended our investigations to CVD growth for large size MLG using quartz and nickel as a support substrate. Figure 3a displays the optical images of transferred top-surface graphene, showing the presence of large size MLG domains for Cu/quartz, after 120 minutes of CVD growth. Although the top surface is covered completely by SLG within 20 minutes, along with very few small MLG domains (supplementary Figure S5), the MLG domains continue to grow larger with extended CVD growth for 2 hours. The MLG domains continued to grow even after the complete coverage of top surface, once again rules out the possibility that top surface is the only origin for nucleation of MLG, rather involves the other sources. Nevertheless, Figure 3b reveals that graphene film persists to be MLG-free uniform monolayer for Cu/nickel configuration even though for extended growth to 120 minutes. Figure 3c,d illustrate the Raman spectra acquired from marked areas indicate the features of MLG for Cu/quartz and uniform SLG for Cu/nickel configuration.[35] The Raman images is constructed by using FWHM (full width at half maximum) of the 2D band, evidencing the uniform SLG growth (FWHM ~24-32 cm^{-1})[35, 37] on the Cu/nickel sample whilst presence of MLG domains (FWHM > 50 cm^{-1}) for the Cu/quartz system, as evident from Figure 3 e,f. In addition, the absence of graphene on the backside of the Cu foil for Cu/nickel case (supplementary Figure S6), identifies the role of the nickel support as backside carbon gettering (BCG) to limit the bulk diffusion through Cu, resulting in a lack of MLG nucleation on the top surface. To

further confirm the role of carbon diffusion from the backside of Cu foil for MLG growth, we carried out CVD growth by wrapping/sealing the Cu foil around the quartz substrate to close the possible gaps for leaking-in the gas precursors to the back surface, as a control experiment. The growth resulted in uniform SLG on the top side, while no growth on the backside of Cu foil, shown in supplementary Figure S7, similar to the aforementioned BCG method. Additionally, we tune the gap size to see the BCG effect by maintaining a gap of 0.5 mm and 2.0 mm between nickel support and Cu foil, shown in Figure S8. Interestingly, by increasing the gap from 0.5 to 2 mm, the MLG patches start to appear again indicating the BCG effect is diminishing. These findings cement our proposed mechanism of subsequent suppression of MLG nucleation through gettering the carbon from the backside of the Cu foil.

To deeply understand the mechanism of BCG graphene growth, we analyze the chemical nature of the substrates using Time-of-Flight Secondary Ion Mass Spectrometry (ToF-SIMS). In this experiment, the same Cu foil was partially supported (right half) with Ni and the rest (left half) with quartz substrate during CVD growth. The Cu foil was slightly oxidized after CVD growth to visualize their boundary, followed with ToF-SIMS ions to map different possible ions. Figure 4a shows ToF-SIMS mapping which illustrates the lack of C^{2-} ions on Cu surface (right half) supported with Ni substrate, indicating the absence of C species or graphene,[38] in contrast to the surface supported with quartz (left half). Besides, lack of CuO_2^- ions on the left half specifies the oxidation barrier provided by graphene film on subsequent Cu surface. It is worth noticing that we did not find any Ni ions on the backside of Cu foil exhibiting lack of any alloying/welding between Cu and Ni substrate. Furthermore, depth profiling of nickel support substrate before and after CVD growth reflects the penetration of C inside the nickel support during the CVD process, as shown in Figure 4b. The enhanced C concentration inside the nickel support indicates the BCG role of nickel to suppress the carbon diffusion toward the top side of Cu foil during the CVD process. When we replaced the supposedly inert support substrate (quartz) with Ni, the consumption of dissociated C predominantly by the underlying nickel support resulted in a lack of C diffusion upwards to the top surface of Cu.

Although, it is well known that nickel has a higher solubility of carbon as compared to that of Cu,[39] but it does not explain the selective adsorption of carbon species on nickel surfaces during CVD,[40] as we observed the complete absence of graphene on the backside of Cu foil (Figure 1h & 4a). Therefore, we performed density functional theory (DFT) calculations for our system, using the Vienna Ab-initio Simulation Package (VASP)[41] with projector augmented wave (PAW) pseudopotentials,[42] and the Perdew-Burke-Ernzerhof (PBE) exchange-correlation functional.[43] Ni or Cu is modeled by a slab with 6 layers and 5×5 surface supercell. 400 eV is used for the plane-wave cut-off energy, and the systems are fully relaxed until the final force on each atom was < 0.01 eV/Å. 5×5×1 Monkhorst-Pack k-points are sampled over the Brillouin zone. We find that Ni provides preferential binding sites (< 1eV) for C compared with Cu, as shown in Figure 4c, which offers a thermodynamic driving force for C to diffuse towards nickel rather than Cu, in agreement with our experimental findings of BCG outcome. Interestingly, the most energetically favorable site is located at the sub-surface of Ni (see Figure 4c for comparison of the energetics of C at different sites of Ni and Cu). This seems to be consistent with the SIMS depth profile, which reflects the penetration of C near the surface, after CVD growth.

Moreover, we observe that the BCG approach seems to be more effective controlling the nucleation density during the oxygen assisted graphene growth.[9, 29] Figure 5a shows the schematic that how BCG works during the single crystal growth. The backside carbon diffusion (white arrows) for Cu/quartz contributes to increased nucleation density at the top surface of Cu foil, due to higher carbon content at the Cu surface promotes the nucleation of graphene domains.[44] In contrast, BCG mechanism limits the carbon diffusion to the top surface (red arrow) for Cu/nickel, restricting the nucleation density at the top. Figure 5b depicts the plot for nucleation density of graphene domains grown on the top surface of Cu foil supported by quartz, nickel plate (Ni-P) and nickel foam (Ni-F). The nucleation density decreases two orders of magnitude by just replacing quartz with the Ni foam as a support, using same CVD conditions, also shown in Figure S9. It is worth noting that no chemical/electropolishing of Cu foil before CVD growth is needed in our processes. Yet, the nucleation density reaches to as low as 6.11 nuclei/cm^2 (0.06 nuclei/mm^2) for Cu/Ni foam, which is among the lowest reported so far.[7, 9-11, 31] Interestingly, oxygen presence accelerates the carbon diffusion through the bulk Cu,[20] therefore, suppressing the carbon diffusion thus favors the process. This approach is very unique and seldom reported to control the nucleation density on the top surface of the Cu foil while operating from the backside, in contrast to the previously reported merely top-surface based modifications.[8-10, 12, 28, 31]

Figure 5(c-e) shows the SEM images of graphene domains grown on Cu foil using different support substrates, the growth time was 10 minutes for (c) and 60 minutes for (d & e). Interestingly, we also observed that using Ni foam instead of Ni plate also lowers down the nucleation density from 44.3 nuclei/cm^2 to 6.11 nuclei/cm^2, at same conditions. This event can be explained by the fact of amplified carbon gettering capability of Ni foam with more surface, and creating a deficiency of active carbon species in the local environment, with higher catalytic power for carbon precursors competing with the subsequent Cu surface, as verified with our DFT calculations discussed above. Figure 5f plot domain size as a function of growth time, using three different support substrate. For Cu/quartz, the domain size is limited to 361 μm on untreated Cu foil since high nucleation density resulted in merging of domains within 30 minutes of growth. Conversely, Ni plate and further Ni foam facilitate growing large millimeter-sized domains of single crystal graphene assisted by low nucleation density achieved through BCG effect. For Cu/Ni foam, graphene domains with ~ 4.5 mm lateral size was grown within 5 hours (15 μm/min) of CVD, which is considered as the fast growth for millimeter-sized domains on Cu foil.[30, 40, 45] However, decreasing the flow rate of methane produces single crystal domain of 6 mm in lateral size on Cu/Ni foam (inset Figure 5f) with growth rate of 10 μm/min, faster than conventional CVD method.[7-11, 31] Further, we verified the single crystal nature of large graphene domains by performing selected area electron diffraction (SAED) on transferred domain to TEM grid. SAED patterns were taken from more than 20 random spots over the 3 mm domain; the same orientation of these patterns with rotation less than 1.5 degrees indicated the single crystallinity of the graphene, as shown in Figure S10. Figure 5g shows the photograph of as grown isolated single crystal graphene domains on Cu/Ni foam, after oxidation for the visualization. Figure 5h depicts the domains transferred to the 2 cm×2 cm SiO_2/Si wafers. Furthermore, Figure 5i shows optical image revealing the benefit of BCG method to get large single crystal graphene domains free of any bi-multilayer graphene patches, which

otherwise observed for Cu/quartz shown in Figure 5j and also in most of the literature reported previously.[7, 10, 11, 31]

Finally, we implemented our BCG approach to grow MLG-free uniform large area continuous SLG sheet crucial for efficient optoelectronic devices. Herein, we demonstrate the graphene growth on "untreated" Cu foil using quartz and nickel as a support substrate, respectively. Figure 6a shows the optical images revealing the presence of aligned MLG patches underneath the SLG film grown on Cu/quartz, analogous to rolling features present on raw Cu foil (supplementary Figure S11). On the other hand, we get exclusively uniform SLG on Cu/nickel within 30 minutes of CVD growth using the BCG method, without any observable MLG patches over the area of 2 cm×2 cm, as shown in Figure 6b and S12. Furthermore, it is worth noticing that our BCG method allows the total elimination of the complicated surface pretreatment step conventionally required for graphene growth.[13, 15, 18] Achieving large area MLG-free uniform SLG on Cu foil, without any prior surface treatment (chemical/electro-polishing) is useful particularly for industrial applications.

To evaluate the electronic properties, we fabricate the FET devices into Hall bar geometry using electron beam lithography and oxygen plasma etching, as shown in Figure 6c. The resistivity (ρ_s) is plotted as a function of gate voltage (V) and Hall mobility is measured by fitting the data for continuous graphene synthesized using conventional (Cu/quartz) and BCG (Cu/nickel) CVD method, as depicted in Figure 6d. The field-effect mobility of electron and holes is represented by blue and red fitted curves, respectively. For graphene synthesized by conventional CVD, the field effect curve seems highly distorted and doped as compared to that of synthesized by BCG method. Moreover, the mobility of graphene synthesized by BCG method has improved substantially and reaches to 6800 $cm^{-2}V^{-1}S^{-1}$ for electrons, which is 2.6 times higher than graphene grown on Cu/quartz (2600 $cm^{-2}V^{-1}S^{-1}$). The remarkable improvement in electrical transport properties can be attributed to the complete removal of MLG patches using our novel method.[18, 46] Further improvements in mobility values may also be achieved by optimizing the transfer method through reducing the effect of contaminations.[20, 29] Nevertheless, our method provides an additional advantage to omit the extra step of removing backside graphene on Cu foil,[7] which resulted in more efficient and cleaner transfer using wet transfer method, as shown in supplementary Figure S13. Furthermore, we transferred graphene films on the glass to evaluate the transmittance of SLG grown by the conventional and BCG method, as shown in Figure 6e. At 550 nm wavelength, the measured transmittance was 97.7% and 96.1% for SLG grown on Cu/nickel and Cu/quartz, respectively. Lower attenuation of transmitted light (2.3%) for graphene grown by BCG method, reflects the complete elimination of scattering centers (MLG patches). Therefore, our "gettering" CVD method steers the conventional CVD process towards new possibilities to synthesize high-quality exclusive SLG either continuous or large single crystal domains for scaling up the potential graphene-based transparent and high-performance optoelectronic devices.

Conclusion

In conclusion, we insight deeply into the origin of multilayer graphene nucleation by adopting the strategy of using a "gettering" substrate during the CVD process. Our results indicate graphene growth on the top surface is strongly depended on the back surface of Cu foil that pursues with carbon diffusion through bulk Cu. By shutting down the carbon

supply from backside to the top surface, with the introduction of nickel substrate as a getter, we were able to completely suppress the nucleation of MLG and single crystal domains. Furthermore, this BCG approach implemented successfully to reduce the nucleation density by two orders of magnitude, which allow us to grow very large single crystal graphene. Furthermore, with our method, prior surface treatment is not required to obtain large area exclusively SLG with high carrier mobility and transmittance.

Materials and Methods

Continuous Graphene growth *via* chemical vapor deposition (CVD)

Cu foil (99.8%) with 25 µm thickness was purchased from Alfa Aesar, Product No. 46365. It is worth noting that we did not use any chemical/electropolishing step for graphene growth on Cu foil. Further, we used three substrates to support the Cu foil inside the CVD furnace; 1) quartz 2) quartz(Cu) 3) nickel plate. In order to get quartz(Cu) substrate, we run the CVD system to anneal Cu foil resting on a fresh quartz substrate (usually used for CVD) for a number of cycles at 1050 ˚C, resulting in Cu evaporation on a quartz substrate. After putting the Cu foil on a typical support substrate, loaded inside quartz tube (2.54 cm diameter) enclosed by tube furnace. The 350 sccm of Ar gas (Hong Kong Specialty Gases Co., Ltd., 99.999%, oxygen concentration <3 ppm) purged inside for 10 minutes to expel all the air inside the reaction chamber. Thereafter, The Cu foil heated to 1050 ˚C under the flow of 350 sccm Ar gas and 16 sccm H_2 gas (Hong Kong Specialty Gases Co., Ltd., 99.999%, oxygen concentration <5 ppm), followed by annealing at same conditions for 20 minutes. Finally, the graphene growth commenced by introducing 16 sccm CH_4 (500 ppm diluted in argon, Arkonic Gases and Chemicals Inc., 99.99%) for a certain time of growth. After growth, the furnace switched off and slide downstream for rapidly cool the samples to room temperature under protecting Ar gas environment. The growth conditions were kept the same for all of three support substrates for sake of comparison.

Large size Bi-multilayer graphene (B/MLG) growth *via* CVD

The 25 µm Cu foil (46365) was cleaned with acetic acid for 5 minutes followed by rinsing in DDI water and blow dried in N_2 atmosphere. The cleaned Cu foil heated to 200 ˚C at the heating plate in ambient conditions to passivate the Cu, subsequently put on a typical support substrate and loaded inside the CVD chamber. The Cu foil heated to 1050 ˚C underflow of 350 sccm of Ar gas only, followed by annealing for 20 minutes with the addition of 15 sccm of H_2 to gas streams. The B/MLG growth initiated with the introduction of 16 sccm (500 ppm diluted in Ar) CH_4 to the flow for a certain growth period, thereafter shutting down the furnace and rapid cooling as described above.

Single crystal graphene growth *via* CVD

As received commercial Cu foil (46365) with 25 µm thickness was pre-oxidized to 210 ˚C at the heating plate in the air and placed on quartz/nickel plate/ nickel foam substrate. The stack is loaded in CVD furnace. The Cu foil heated to growth temperature 1050 ˚C under a flow of 350 sccm of Ar gas only, followed by annealing for 20 minutes with the addition of 22 sccm of H_2 to gas streams. The single-crystal graphene domains grown with the introduction of 13 sccm CH_4 (500 ppm diluted in Ar) to the flow for a predetermine growth time, thereafter shutting down the furnace and rapid cooling as described above.

Graphene transfer to 300 nm SiO_2/Si substrate

After a typical CVD growth, the Cu foil with graphene on top was coated with 300 nm thick PMMA by spin coating (3000 rpm/30 sec), followed by baking at 150 ˚C for 5 minutes to cure it. The PMMA coated graphene/ Cu foil floated on etchant solution (10g $FeCl_3$, 10 ml HCl and 200ml DI water) to etch away the Cu for approx. 5 hours. The transparent PMMA/graphene stack then transferred to diluted HCl solution to remove all the etchant residues, subsequently rinsed with DI water thrice. The cleaned PMMA/ graphene stack scoped up on 300 nm SiO2/Si wafers and dried at 70 ˚C for 20 minutes. Finally, the wafers were exposed to acetone vapors to remove the PMMA.

Characterization of graphene and support substrates

X-ray diffraction patterns were obtained through multipurpose Empyrean (PANanalytical) X-ray diffraction, operated in thin film mode (Cu Kα radiation, 40 kV, 30 mA, grazing incidence at 1°). Optical micrographs of samples were taken using LEICA DMLM optical microscope integrated with LEICA DFC 290 camera. ImageJ software was used to analyze the micrographs for graphene domain size and coverage. The Cu foil after CVD growth was oxidized in air at 200 ˚C for 1 minute to visualize graphene on both sides of Cu foil.

Raman spectra were taken by InVia micro-Raman system (Renishaw) equipped with Ar+ ion laser 514.5 nm excitation laser sources. A 50× objective lens was used to focus the laser beam. Depth profiling of Ni substrate before and after CVD was performed by time-of-flight secondary ion mass spectrometer (ION-TOF GmbH) using 3 KeV-Cs^+ as sputter source and 25 KeV-Bi_3^+ as analysis source for SIMS mapping of Cu foil.

Device fabrication and carrier mobility measurement

The CVD grown graphene is first etched into Hall bar geometry, by using the oxygen plasma. The metal Ti (10 nm)/ Au (50 nm) is then deposited to form electrodes. The graphene sample is then transferred into Physical Properties Measurement System (PPMS Quantum Design), followed by an *in situ* annealing, with temperature fixed at 390 K for 1.5 hours. The temperature is then cool down to 20 K for electronic transport measurement. The resistivity is plotted as a function of gate voltage. The data can be fitted by using the formula

$$\rho = \rho_s + \frac{1}{\mu e\sqrt{\left(CV/e\right)^2 + n_0^2}},$$

where e is the elementary charge, C is the capacitance per unit area for SiO_2, ρ_s is the resistivity caused by short-range scatterings, μ is the mobility governed by long-range scattering, n_0 is the residue charged carrier density arising from the electron-hole puddles in graphene. Since an asymmetry behavior is observed between electron and hole sides, we fit the data separately for these two sides. The fitting results are plotted by solid curves, with the red for holes side and blue for electrons side.

Acknowledgements

This project is supported by the Research Grant Council of Hong Kong SAR (Project number 16204815). We appreciate the support from Center for 1D/2D Quantum Materials and the Innovation and Technology Commission (ITC-CNERC14SC01). I.H.A. appreciate financial support from Higher Education Commission (HEC) of Pakistan. Technical assistance from

the Materials Characterization and Preparation Facilities is greatly appreciated. Y.L. thanks the support from Resnick Prize Postdoctoral Fellowship at Caltech. WAG thanks, NSF (DMREF-1436985) and DOE (DE-SC0014607) for support. This work used computational resources of National Energy Research Scientific Computing Center, a DOE Office of Science User Facility supported by the Office of Science of the U.S. DOE under Contract DE-AC02-05CH11231, the Extreme Science and Engineering Discovery Environment (XSEDE), which is supported by NSF Grant ACI-1053575, and of National Renewable Energy Laboratory supported by DoE office of Energy Efficiency and Renewable Energy.

References

1. A. K. Geim and K. S. Novoselov, *Nat Mater*, 2007, **6**, 183-191.
2. X. Li, W. Cai, J. An, S. Kim, J. Nah, D. Yang, R. Piner, A. Velamakanni, I. Jung and E. Tutuc, *Science*, 2009, **324**, 1312-1314.
3. S. Bae, H. Kim, Y. Lee, X. Xu, J.-S. Park, Y. Zheng, J. Balakrishnan, T. Lei, H. Ri Kim, Y. I. Song, Y.-J. Kim, K. S. Kim, B. Ozyilmaz, J.-H. Ahn, B. H. Hong and S. Iijima, *Nat Nano*, 2010, **5**, 574-578.
4. X. Li, L. Colombo and R. S. Ruoff, *Advanced Materials*, 2016, n/a-n/a.
5. P. Y. Huang, C. S. Ruiz-Vargas, A. M. van der Zande, W. S. Whitney, M. P. Levendorf, J. W. Kevek, S. Garg, J. S. Alden, C. J. Hustedt, Y. Zhu, J. Park, P. L. McEuen and D. A. Muller, *Nature*, 2011, **469**, 389-392.
6. G.-X. Ni, Y. Zheng, S. Bae, H. R. Kim, A. Pachoud, Y. S. Kim, C.-L. Tan, D. Im, J.-H. Ahn, B. H. Hong and B. Özyilmaz, *ACS Nano*, 2012, **6**, 1158-1164.
7. H. Zhou, W. J. Yu, L. Liu, R. Cheng, Y. Chen, X. Huang, Y. Liu, Y. Wang, Y. Huang and X. Duan, *Nat Commun*, 2013, **4**.
8. L. Gan and Z. Luo, *ACS Nano*, 2013, **7**, 9480-9488.
9. Y. Hao, M. S. Bharathi, L. Wang, Y. Liu, H. Chen, S. Nie, X. Wang, H. Chou, C. Tan, B. Fallahazad, H. Ramanarayan, C. W. Magnuson, E. Tutuc, B. I. Yakobson, K. F. McCarty, Y.-W. Zhang, P. Kim, J. Hone, L. Colombo and R. S. Ruoff, *Science*, 2013, **342**, 720-723.
10. W. Guo, F. Jing, J. Xiao, C. Zhou, Y. Lin and S. Wang, *Advanced Materials*, 2016, **28**, 3152-3158.
11. J. Li, X.-Y. Wang, X.-R. Liu, Z. Jin, D. Wang and L.-J. Wan, *Journal of Materials Chemistry C*, 2015, **3**, 3530-3535.
12. Z. Yan, J. Lin, Z. Peng, Z. Sun, Y. Zhu, L. Li, C. Xiang, E. L. Samuel, C. Kittrell and J. M. Tour, *ACS Nano*, 2012, **6**, 9110-9117.
13. J. Pang, A. Bachmatiuk, L. Fu, C. Yan, M. Zeng, J. Wang, B. Trzebicka, T. Gemming, J. Eckert and M. H. Rummeli, *The Journal of Physical Chemistry C*, 2015, **119**, 13363-13368.
14. H. C. Lee, S. B. Jo, E. Lee, M. S. Yoo, H. H. Kim, S. K. Lee, W. H. Lee and K. Cho, *Advanced Materials*, 2016, **28**, 2010-2017.
15. Z. Luo, Y. Lu, D. W. Singer, M. E. Berck, L. A. Somers, B. R. Goldsmith and A. T. C. Johnson, *Chemistry of Materials*, 2011, **23**, 1441-1447.

16. A. Mohsin, L. Liu, P. Liu, W. Deng, I. N. Ivanov, G. Li, O. E. Dyck, G. Duscher, J. R. Dunlap, K. Xiao and G. Gu, *ACS Nano*, 2013, **7**, 8924-8931.

17. E. Rezvani, T. Hallam, N. McEvoy, N. C. Berner and G. S. Duesberg, *Carbon*, 2015, **95**, 789-793.

18. Z. Han, A. Kimouche, D. Kalita, A. Allain, H. Arjmandi-Tash, A. Reserbat-Plantey, L. Marty, S. Pairis, V. Reita, N. Bendiab, J. Coraux and V. Bouchiat, *Advanced Functional Materials*, 2014, **24**, 964-970.

19. W. Fang, A. L. Hsu, Y. Song, A. G. Birdwell, M. Amani, M. Dubey, M. S. Dresselhaus, T. Palacios and J. Kong, *ACS Nano*, 2014, **8**, 6491-6499.

20. Y. Hao, L. Wang, Y. Liu, H. Chen, X. Wang, C. Tan, S. Nie, J. W. Suk, T. Jiang, T. Liang, J. Xiao, W. Ye, C. R. Dean, B. I. Yakobson, K. F. McCarty, P. Kim, J. Hone, L. Colombo and R. S. Ruoff, *Nat Nano*, 2016, **11**, 426-431.

21. W. Fang, A. Hsu, Y. C. Shin, A. Liao, S. Huang, Y. Song, X. Ling, M. S. Dresselhaus, T. Palacios and J. Kong, *Nanoscale*, 2015, **7**, 4929-4934.

22. Z. Zhao, Z. Shan, C. Zhang, Q. Li, B. Tian, Z. Huang, W. Lin, X. Chen, H. Ji, W. Zhang and W. Cai, *Small*, 2015, **11**, 1418-1422.

23. N. Shu, W. Wei, X. Shirui, Y. Qingkai, B. Jiming, P. Shin-shem and F. M. Kevin, *New Journal of Physics*, 2012, **14**, 093028.

24. L. Gan, H. Zhang, R. Wu, Q. Zhang, X. Ou, Y. Ding, P. Sheng and Z. Luo, *Nanoscale*, 2015, **7**, 2391-2399.

25. Q. Li, H. Chou, J.-H. Zhong, J.-Y. Liu, A. Dolocan, J. Zhang, Y. Zhou, R. S. Ruoff, S. Chen and W. Cai, *Nano Letters*, 2013, **13**, 486-490.

26. P. Wu, X. Zhai, Z. Li and J. Yang, *The Journal of Physical Chemistry C*, 2014, **118**, 6201-6206.

27. B. Wang, M. Huang, L. Tao, S. H. Lee, A. R. Jang, B.-W. Li, H. S. Shin, D. Akinwande and R. S. Ruoff, *ACS Nano*, 2016, **10**, 1404-1410.

28. L. Lin, J. Li, H. Ren, A. L. Koh, N. Kang, H. Peng, H. Q. Xu and Z. Liu, *ACS Nano*, 2016, **10**, 2922-2929.

29. X. Xu, Z. Zhang, L. Qiu, J. Zhuang, L. Zhang, H. Wang, C. Liao, H. Song, R. Qiao, P. Gao, Z. Hu, L. Liao, Z. Liao, D. Yu, E. Wang, F. Ding, H. Peng and K. Liu, *Nat Nano*, 2016, **advance online publication**.

30. S. Wang, H. Hibino, S. Suzuki and H. Yamamoto, *Chemistry of Materials*, 2016, **28**, 4893-4900.

31. S. Chen, H. Ji, H. Chou, Q. Li, H. Li, J. W. Suk, R. Piner, L. Liao, W. Cai and R. S. Ruoff, *Advanced Materials*, 2013, **25**, 2062-2065.

32. C. Jia, J. Jiang, L. Gan and X. Guo, *Scientific Reports*, 2012, **2**, 707.

33. C. Yang, T. Wu, H. Wang, G. Zhang, J. Sun, G. Lu, T. Niu, A. Li, X. Xie and M. Jiang, *Small*, 2016, **12**, 2009-2013.

34. P. Blake, E. W. Hill, A. H. Castro Neto, K. S. Novoselov, D. Jiang, R. Yang, T. J. Booth and A. K. Geim, *Applied Physics Letters*, 2007, **91**, 063124.

35. A. C. Ferrari, J. C. Meyer, V. Scardaci, C. Casiraghi, M. Lazzeri, F. Mauri, S. Piscanec, D. Jiang, K. S. Novoselov, S. Roth and A. K. Geim, *Physical Review Letters*, 2006, **97**, 187401.

36. H. Kim, C. Mattevi, M. R. Calvo, J. C. Oberg, L. Artiglia, S. Agnoli, C. F. Hirjibehedin, M. Chhowalla and E. Saiz, *ACS Nano*, 2012, **6**, 3614-3623.

37. D. Graf, F. Molitor, K. Ensslin, C. Stampfer, A. Jungen, C. Hierold and L. Wirtz, *Nano Letters*, 2007, **7**, 238-242.

38. H. Chou, A. Ismach, R. Ghosh, R. S. Ruoff and A. Dolocan, *Nat Commun*, 2015, **6**.

39. K. S. Kim, Y. Zhao, H. Jang, S. Y. Lee, J. M. Kim, K. S. Kim, J.-H. Ahn, P. Kim, J.-Y. Choi and B. H. Hong, *Nature*, 2009, **457**, 706-710.

40. D. Ding, P. Solís-Fernández, H. Hibino and H. Ago, *ACS Nano*, 2016.

41. G. Kresse and J. Furthmüller, *Phys. Rev. B*, 1996, **54**, 11169-11186.

42. P. E. Blöchl, *Phys. Rev. B*, 1994, **50**, 17953-17979.

43. J. P. Perdew, K. Burke and M. Ernzerhof, *Phys. Rev. Lett.*, 1996, **77**, 3865-3868.

44. P. Braeuninger-Weimer, B. Brennan, A. J. Pollard and S. Hofmann, *Chemistry of Materials*, 2016.

45. L. Lin, L. Sun, J. Zhang, J. Sun, A. L. Koh, H. Peng and Z. Liu, *Advanced Materials*, 2016, **28**, 4671-4677.

46. T. Ohta, A. Bostwick, J. L. McChesney, T. Seyller, K. Horn and E. Rotenberg, *Physical Review Letters*, 2007, **98**, 206802.

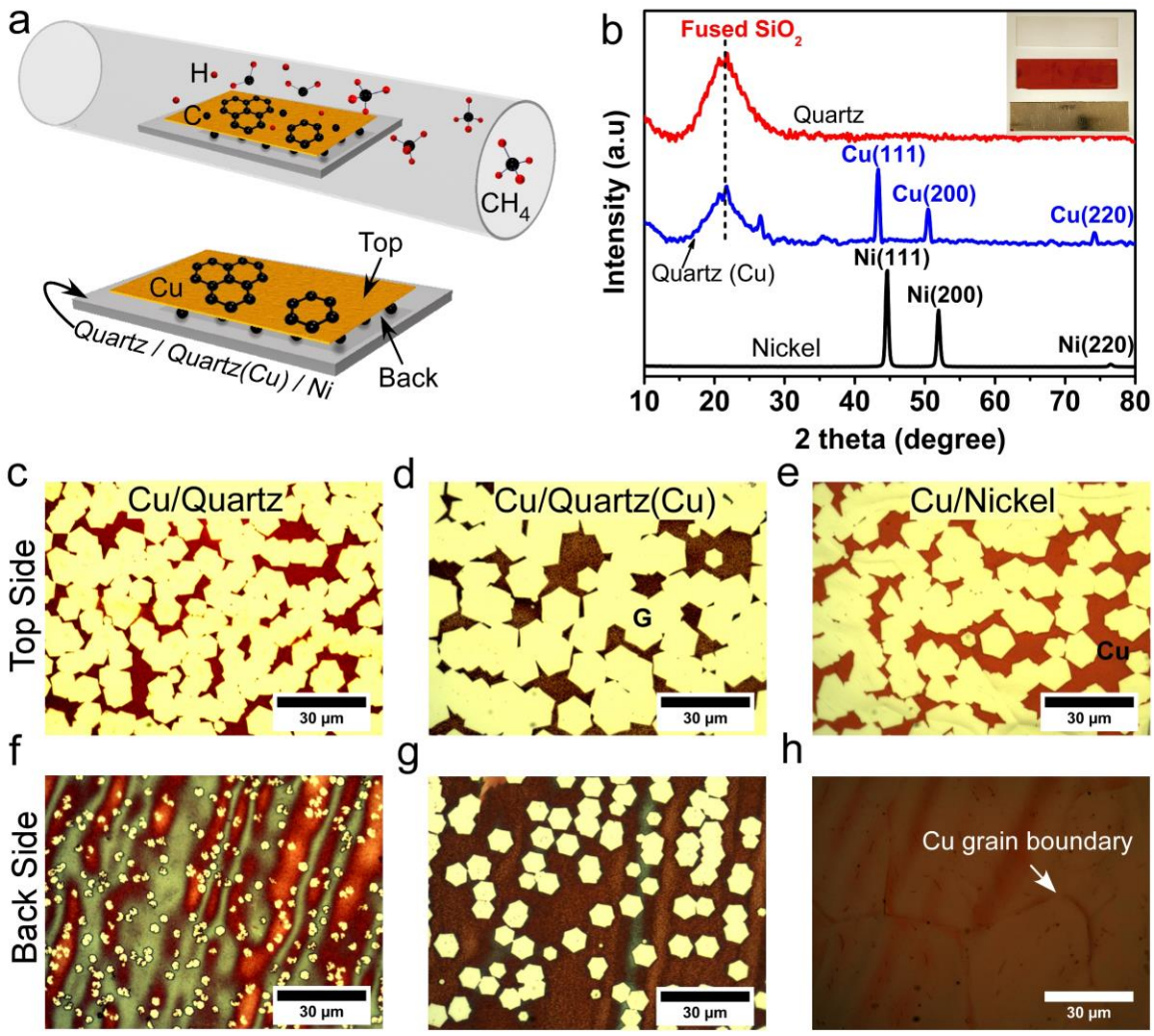

Figure 1. CVD graphene growth on Cu foil using different support substrates. (a) Schematic illustrating CVD growth on Cu foil using three support substrates *i.e*, quartz, quartz(Cu) and nickel. Graphene growth on the top and backside of the Cu foil (indicated by arrows) is studied in this work. (b) XRD spectra of three support substrates. In case of quartz(Cu) the presence of Cu peaks in addition to fused silica, reflects the Cu evaporation on fresh quartz substrate. Optical images of CVD graphene growth for 5 minutes on (c-e) top surface and (f-h) back surface of Cu foil using quartz (c,f), quartz(Cu) (d,g) and nickel (e,h) as a support substrate, respectively. Although, graphene growth is almost similar on top side of Cu foil in all cases but far different on backside. The graphene growth completely suppressed on backside of Cu foil while using nickel as support substrate (h). Cu foil was oxidized in air at 200 ˚C for 5 minutes after growth for optical visualization.

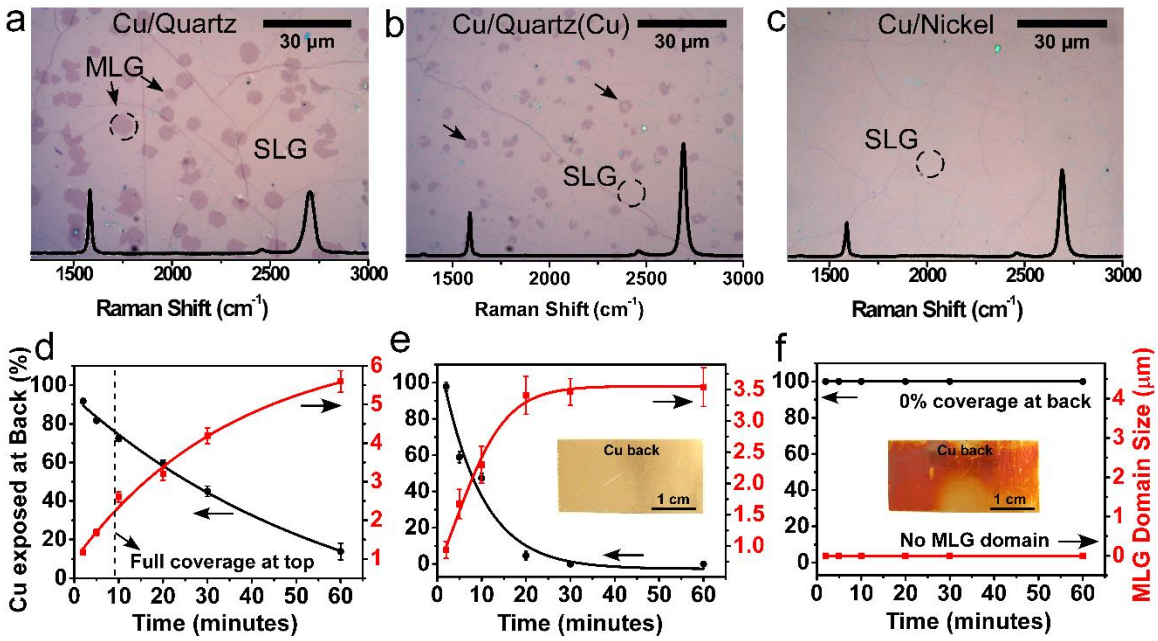

Figure 2. Transferred graphene grown on top surface and correlation between growth on top and backside. Optical images of graphene transferred to SiO_2/Si substrate from top surface of Cu foil after 60 minutes of CVD using quartz (a) quartz(Cu) (b) and nickel (c) as supporting substrate. Multilayer graphene (MLG) domains were observed in a,b marked with arrows, while for Cu/nickel system (c) the film consist of MLG-free single layer graphene (SLG). Representative Raman spectra acquired from marked circles exhibit MLG (a) and SLG (b,c) characteristics. (d-f) Plots showing MLG domains size evolution with CVD growth time and correlating with percentage Cu exposed on backside (percentage graphene coverage). These plots revealed a strong coupling between growth of MLG domains (top surface) and graphene coverage (at back surface). Once the backside of the Cu foil covered completely with graphene (inset shows the backside of Cu foil after CVD), the MLG size become constant for further growth time (e). For case of nickel substrate (f), we did not observe any graphene at backside of Cu foil (inset shows the backside of Cu foil), so as complete absence of MLG domains at top surface.

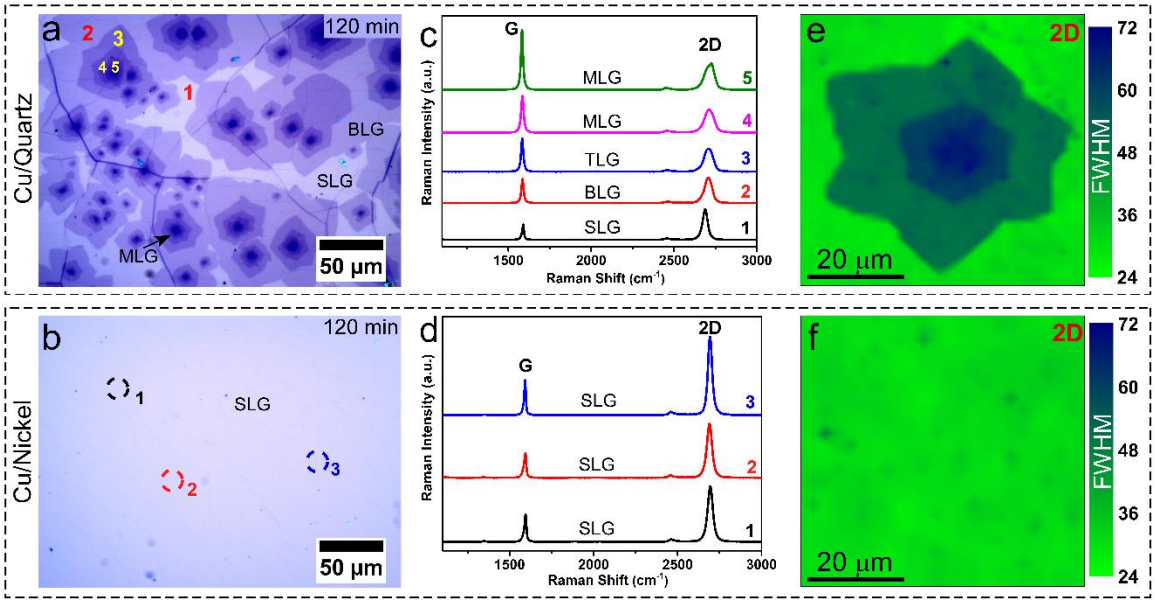

Figure 3. Large size multilayer graphene growth conditions and Raman analysis. (a,b) optical images of CVD graphene grown using multilayer graphene growth conditions with quartz (a) and nickel (b) as support substrate. Graphene grown on Cu/quartz consist of BLG and MLG domains, while totally SLG observed for Cu/nickel configuration. (c,d) Raman spectra acquired from different points marked in optical images. The Raman spectra (c) confirms the MLG presence, but the Raman spectra (d) reflects the SLG characteristics at all acquired points. (e,f) Raman mapping of graphene by FWHM of 2D band. Image (e) shows multilayer graphene distribution of FWHM (>50 cm^{-1}) while image (f) reveals the uniform monolayer graphene (FWHM <32 cm^{-1}).

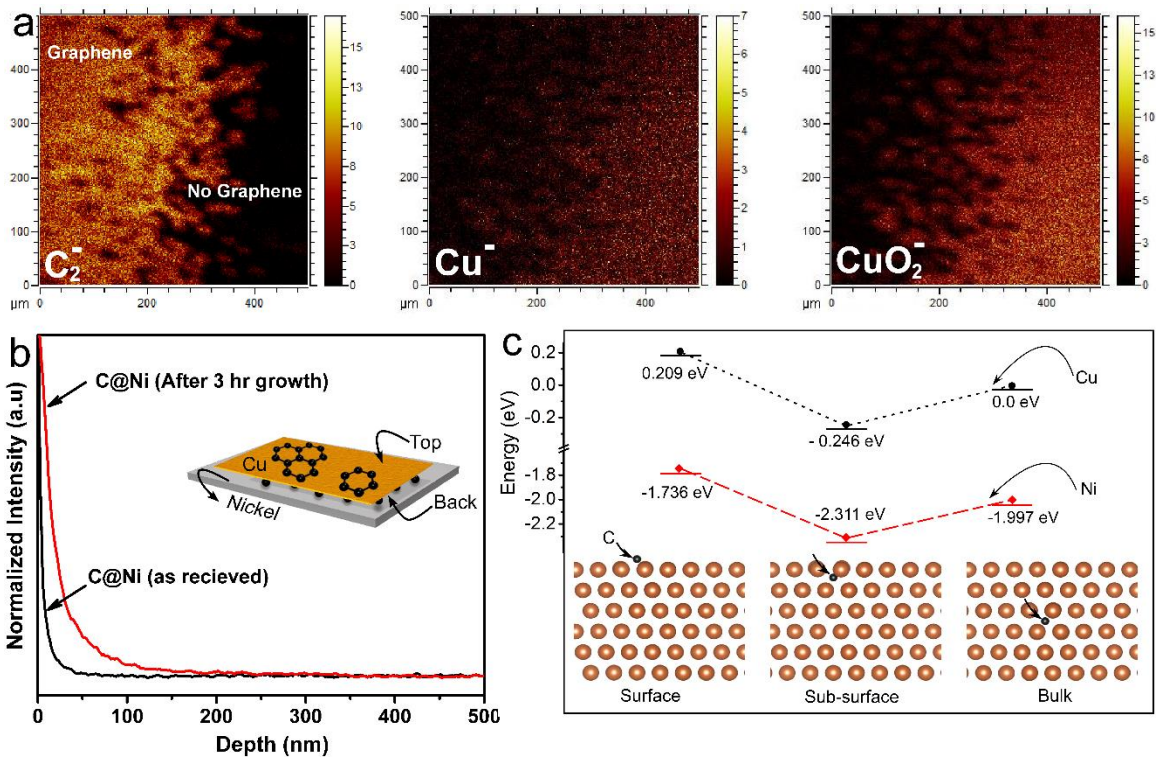

Figure 4. ToF-SIMS analysis of Cu foil and nickel support substrate and Density functional theory (DFT) calculations to explain BCG mechanism. (a) ToF-SIMS mapping of backside of Cu foil supported with right half (left half) with nickel (quartz) during CVD growth. The Cu foil is oxidized after growth to visualize the boundary. The mapping reveals the absence (presence) of carbon species (C_2^-) at area supported with nickel (quartz) substrate (b) Carbon SIMS depth profile on nickel support before and after CVD growth for 3 hours. Higher concentration of carbon in depth of nickel substrate after growth reflects its role for gettering the carbon species at the interface, during CVD growth. (c) Atomic structure and calculated energies of C distribution at different sites of Cu/Ni lattice illustrated (the energy of C at bulk Cu is set to zero as a reference). Ni sub-surfaces provide more energetically favorable sites for C species as compared to Cu, which is consistent with experimental findings.

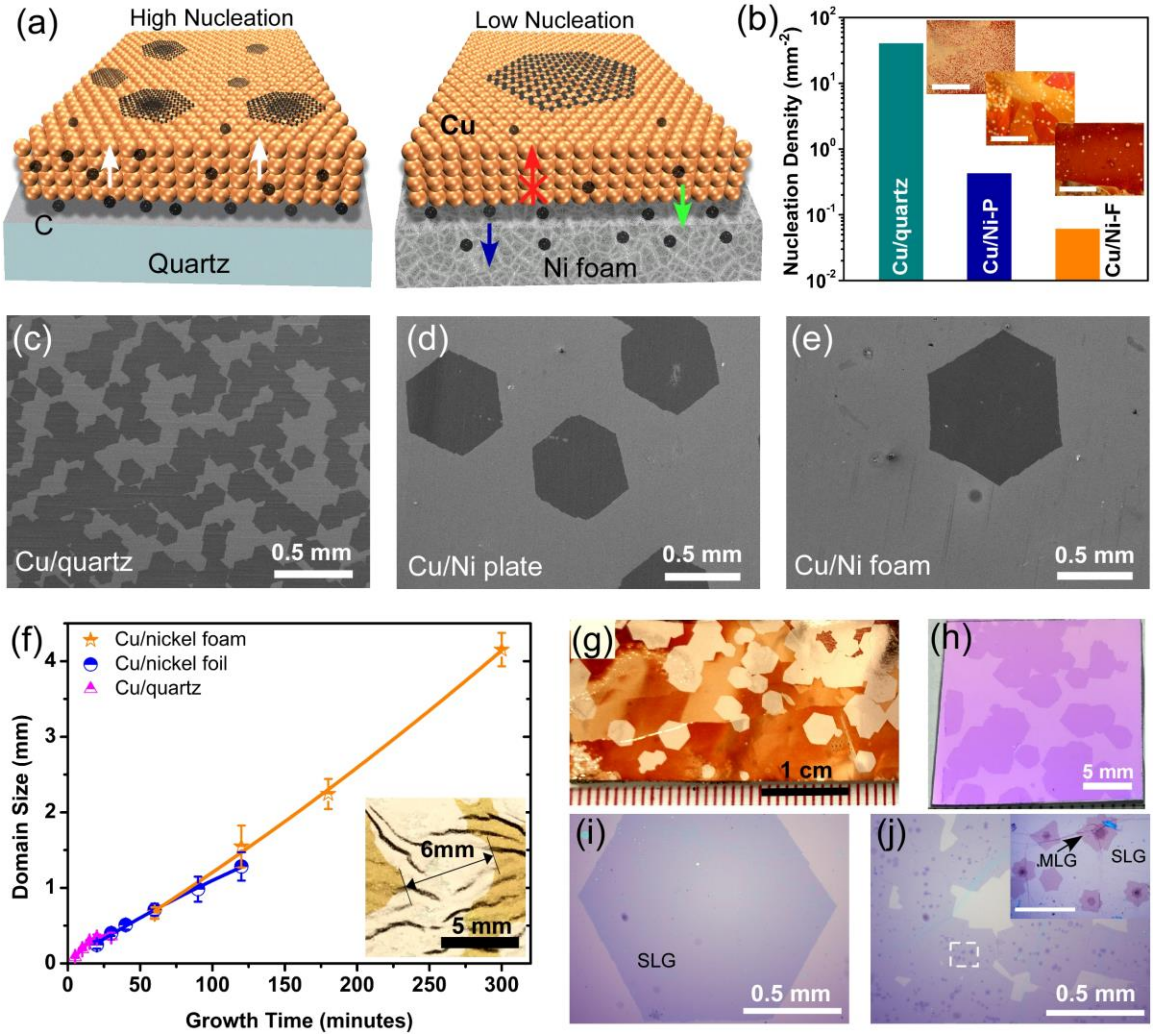

Figure 5. Single crystal graphene growth on untreated Cu foil using quartz, Ni plate and Ni foam as a support substrate. (a) Schematic showing the mechanism of nucleation density control using BCG method. Carbon diffuses from the backside of the Cu foil (white arrows) to enhance the nucleation density at the top surface for Cu/quartz, while using Ni foam as a support triggers the BCG mechanism (blue arrow) which prevents the extra supply of carbon from the backside (red arrow) and dissolving carbon from the top surface of Cu (white arrow). (b) Plot showing nucleation density of graphene domains at the top surface of Cu foil decreases about two orders of magnitude by replacing quartz with Ni-foam as support.(c-e) SEM images of graphene domains grown on Cu foil using three support substrates revealing variance in nucleation density. (f) Shows plot of graphene average domain size with growth time. The size is limited to few hundreds of micron for Cu/quartz as domains merged together within 30 minutes of CVD. While for Cu/Ni foam allows nucleation control to achieve large size single crystal of graphene ~ 4.2 mm for 13 sccm flow rate of CH_4. The inset shows graphene domain of 6mm size. (g-h) Photographs of large single crystals grown on Cu (g) and transferred to SiO_2/Si (h). Optical micrographs revealing the large single crystal exclusive SLG for Cu/nickel (i), and high density of graphene domains for Cu/quartz with enormous MLG domains (inset, scale bar 50 µm).

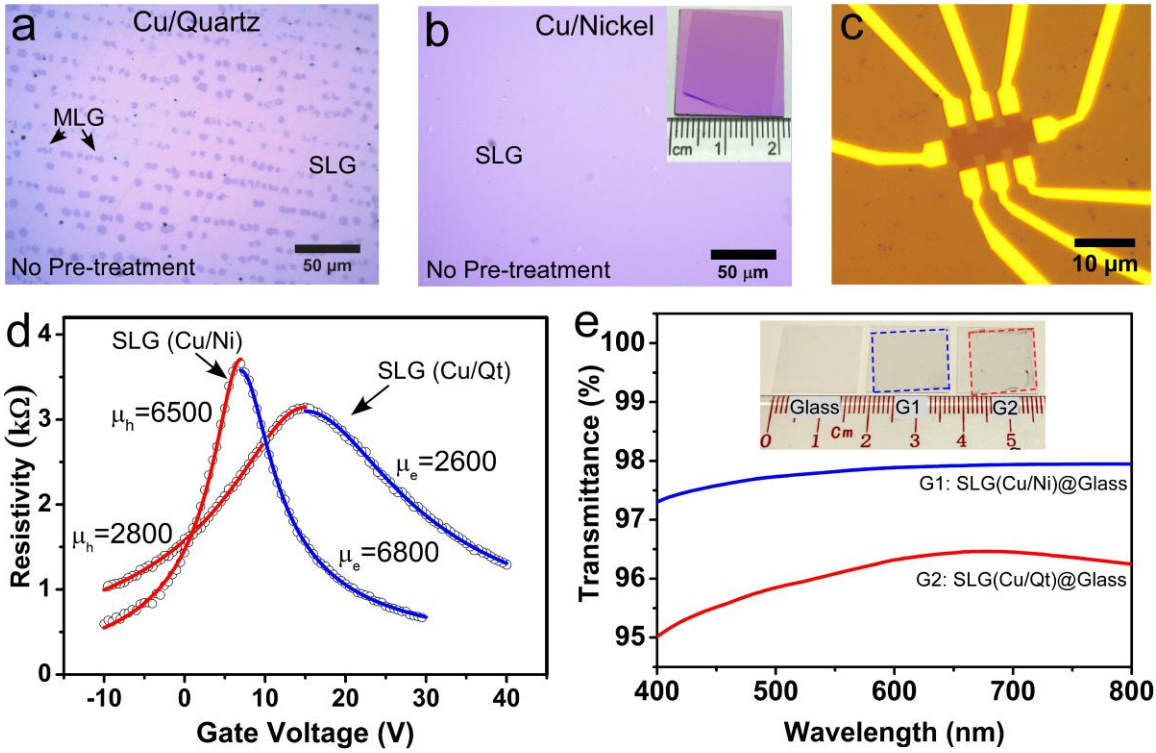

Figure 6. Graphene growth on untreated Cu foil, electrical transport and transmittance measurements. (a,b) Optical images of transferred graphene after CVD growth on untreated Cu foil using quartz (a) and nickel (b) as support substrates. MLG patches are clearly visible for graphene grown on Cu/quartz, while MLG-free SLG revealed grown on Cu/nickel substrate. (c) Optical image of Hall bar configuration of representative FET devices made for carrier mobility measurements. (d) Plots of resistivity against gate voltage of devices fabricated with graphene grown on Cu using quartz and nickel as a support substrate. The carrier mobility of electrons increased to 6800 cm^2/Vs for graphene grown on Cu/nickel, which is 2.6 times higher than graphene grown on Cu/quartz (2600 cm^2/Vs). (e) The transmittance of glass/transferred graphene film grown on Cu/nickel and Cu/quartz, respectively (inset: photographs of graphene transferred samples). Graphene grown by BCG (Cu/Ni) approach shows the higher transmittance of 97.7%, in comparison to 96.1% for graphene (Cu/quartz), measured at 550 nm wavelength.